## PAPER

Check for updates

# Synthesis of cyclic graft polymeric prodrugs with heterogeneous grafts of hydrophilic OEG and reducibly conjugated CPT for controlled release†

Chao Meng,[a,b] Yufei Cao,[b] Lu Sun,[b] Yuping Liu,[b] Guiying Kang,[b] Wei Ma,[b] Jinlei Peng,[b] Kaicheng Deng,[b] Liwei Ma[b] and Hua Wei ⓘ *[a,b]

Fabrication of cyclic graft (*cg*) copolymer-based polymeric prodrugs by conjugation of drug molecules to *cg* copolymers *via* a dynamic covalent bond capable of responding to biorelevant signals integrates simultaneously the merits of *cg* copolymers and polymeric prodrugs for enhanced stability of nanocarriers and precise modulation of drug release kinetics. To completely eliminate the compromised drug conjugation efficiency due to the steric hindrance of hydrophilic grafts, it will be useful to develop *cg* polymeric prodrugs with heterogeneous grafts composed of hydrophilic polymers and drug species, respectively. For this purpose, we reported in this study the synthesis of cyclic graft polymeric prodrugs with heterogeneous grafts of hydrophilic oligo (ethylene glycol) (OEG) and reducibly conjugated camptothecin (CPT), *cg*-poly(oligo(ethylene glycol) monomethyl ether methacrylate)-*b*-poly((2-hydroxyethyl methacrylate)-disulfide link-camptothecin) (*cg*-P(OEGMA)-*b*-P(HEMA–SS–CPT), *cg*-prodrugs), *via* an integrated strategy of a previously reported diblock copolymer-based template and post-polymerization intermolecular click conjugation of a reducible CPT prodrug. The micelles self-assembled from *cg*-prodrugs on one hand had sufficient salt stability due to the branched *cg* structure, and on the other hand showed a reduction-triggered cleavage of the disulfide link for a promoted CPT release. Most importantly, we uncovered two interesting phenomena of the *cg*-based polymeric prodrugs as delivery vehicles: (i) the dimensions of both self-assemblies formed by the *cg* and bottlegraft (*bg*) polymers depend substantially on the molecular size of the *cg* and *bg* polymers likely due to the steric hindrance of the grafted structures of the *cg* and *bg* molecules and relatively low aggregation number of the self-assembled structures, and (ii) *cg*-prodrug-based micelles exhibited greater *in vitro* cytotoxicity against cancer cells despite the lower drug loading content (DLC) than the *bg*-based analogues, which results primarily from the faster reduction-triggered degradation and drug release as well as the greater cellular uptake efficiency of the former micelle prodrugs. Taken together, the developed *cg*-prodrugs provide great potential for chemotherapy, and the aforementioned interesting results will definitely inspire more upcoming studies on the future design and development of novel *cg* polymers for biomedical applications.

[a]*Hunan Province Cooperative Innovation Center for Molecular Target New Drug Study & Department of Pharmacy and Pharmacology, University of South China, Hengyang, 421001, China*
[b]*State Key Laboratory of Applied Organic Chemistry, Key Laboratory of Nonferrous Metal Chemistry and Resources Utilization of Gansu Province, College of Chemistry and Chemical Engineering, Lanzhou University, Lanzhou, Gansu 730000, China. E-mail: weih@lzu.edu.cn, huawei_usc@163.com*

## Introduction

Cyclic graft (*cg*) copolymers with radiating grafts densely attached onto a cyclic core have attracted great research interest in recent years due to their unique topology-generated self-assembly behaviors[1–5] and better performance for potential biomedical applications relative to the bottlegraft (*bg*) analogues.[6–11] The elegant combination of various controlled living radical polymerization (CRP) techniques and intra- and inter-molecular click coupling has enabled the recent rapid development of *cg* copolymers[12–16] with tailor-made structures and compositions based on various polymer species including *cg* copolymers with homogeneous[12,13,15,17–20] and heterogeneous[5,7] grafts. Fabrication of *cg* copolymer-based

polymeric prodrugs by conjugation of drug molecules to the *cg* copolymers *via* a dynamic covalent bond capable of responding to biorelevant signals integrates simultaneously the merits of *cg* copolymers and polymeric prodrugs for enhanced stability of nanocarriers and precise modulation of drug release kinetics. One notable example is Pun's[17] *cg* polymeric prodrugs with homogeneous poly(oligo(ethylene glycol) monomethyl ether methacrylate) (P(OEGMA)) grafts for efficient *in vitro* anticancer drug delivery, but this construct suffered from compromised drug conjugation efficiency and low drug loading capacity of 2–5% due to the steric hindrance of P(OEGMA) grafts. To completely eliminate the negative effect of hydrophilic grafts on drug conjugation, it will be useful to develop *cg* polymeric prodrugs with heterogeneous grafts composed of hydrophilic polymers and drug species, respectively. For this purpose, we reported in this study the synthesis of cyclic graft polymeric prodrugs with heterogeneous grafts of hydrophilic oligo (ethylene glycol) (OEG) and reducibly conjugated camptothecin (CPT), (*cg*-P(OEGMA)-*b*-P(HEMA-SS-CPT), *cg*-prodrugs), *via* an integrated strategy of a previously reported diblock copolymer-based template[7] and post-polymerization intermolecular click conjugation of a reducible CPT prodrug.[21] The self-assembly behaviors and *in vitro* anticancer efficiency of the resulting *cg*-prodrugs were further compared with those of the *bg*-analogues.

## Results and discussion

### Synthesis and characterization of *cg* and *bg*-prodrugs

The preparation of *cg*-prodrug, *cg*-P(OEGMA)-*b*-P(HEMA-SS-CPT), consisted mainly of four steps (Scheme 1): (i) synthesis of a linear precursor, *l*-P(OEGMA)-*b*-P(HEMA)-N$_3$, by successive ATRPs of OEGMA and HEMA and subsequent azidation of the bromine terminus of the synthesized *l*-P(OEGMA)-*b*-P(HEMA)-Br, (ii) intrachain click cyclization of the linear precursor to afford a diblock copolymer-based cyclic template, *c*-P(OEGMA)-*b*-P(HEMA), (iii) conversion of the pendant hydroxyl groups of HEMA units in *c*-P(OEGMA)-*b*-P(HEMA) to highly reactive azide functions by an esterification reaction with 2-bromoisobutyryl bromide (iBuBr), followed by an azidation with sodium azide, and (iv) a reducible CPT prodrug with a disulfide-linked alkynyl terminus denoted as alkynyl-SS-CPT was conjugated to the *cg* copolymer with the azide side groups synthesized in the third step *via* an intermolecular click coupling. The *bg* analogue, *bg*-P(OEGMA)-*b*-P(HEMA-SS-CPT), was synthesized fol-
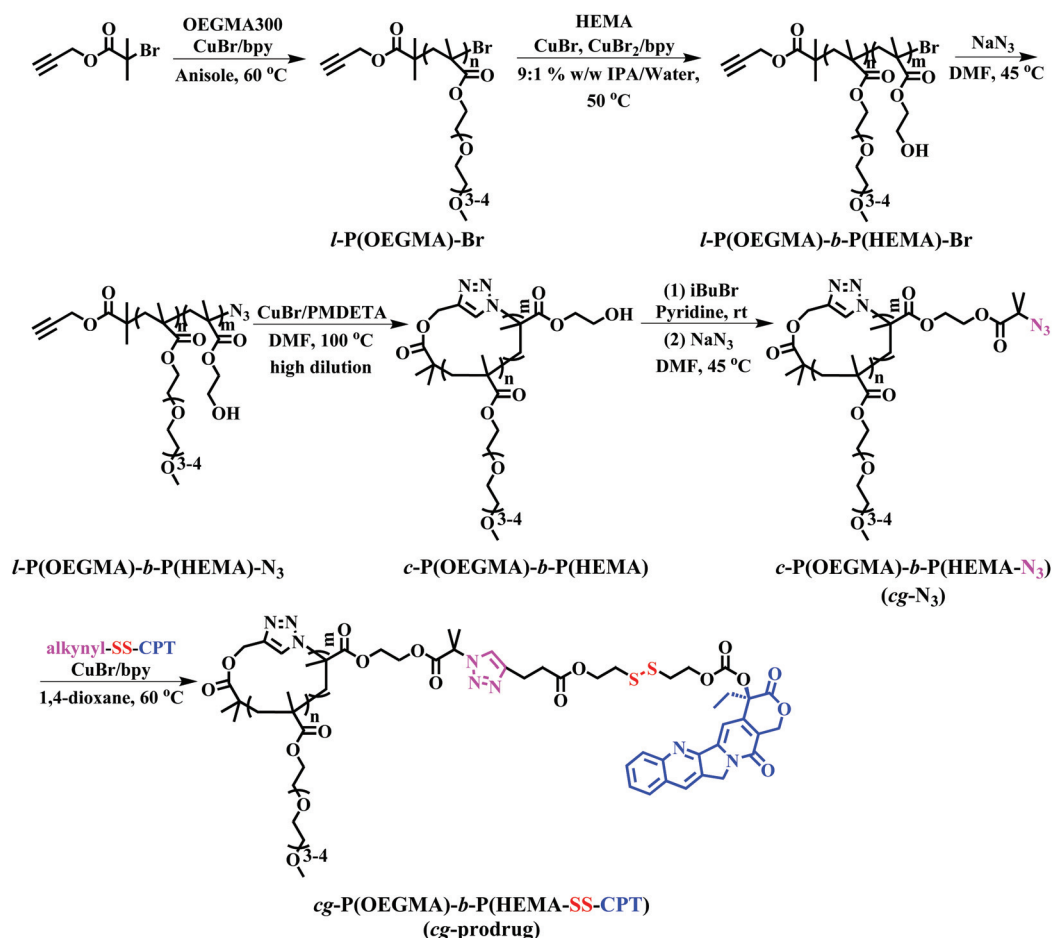


**Scheme 1** Synthesis of *cg*-prodrug.

**Table 1** Summary of *l*-P(OEGMA)-*b*-P(HEMA)-Br prepared by ATRP of HEMA using *l*-P(OEGMA)$_{38}$-Br as a macroinitiator

| Run | Time (min) | DP$^a$ | Conv. (%) | Real structure | $M_w{}^b$ (kDa) | $Đ^b$ |
|---|---|---|---|---|---|---|
| 1 | 30 | 9 | 11.3 | *l*-P(OEGMA)$_{38}$-*b*-P(HEMA)$_9$-Br | 19.1 | 1.1 |
| 2 | 45 | 15 | 18.8 | *l*-P(OEGMA)$_{38}$-*b*-P(HEMA)$_{15}$-Br | 19.8 | 1.1 |
| 3 | 60 | 20 | 25.0 | *l*-P(OEGMA)$_{38}$-*b*-P(HEMA)$_{20}$-Br | 20.4 | 1.1 |
| 4 | 75 | 24 | 30.0 | *l*-P(OEGMA)$_{38}$-*b*-P(HEMA)$_{24}$-Br | 21.2 | 1.1 |

$^a$ Determined by $^1$H NMR analysis. $^b$ Determined by SEC-MALLS.

lowing identical procedures to the aforementioned synthesis of *cg*-prodrug except using ethyl 2-azidoisobutyrate (EAB) end-capped *l*-P(OEGMA)-*b*-P(HEMA)-Br for the drug conjugation in the last step (Scheme S2†).

A precise synthesis of α-alkynyl, ω-azide linear precursors with fully functionalized termini is crucial for the successful synthesis of cyclic polymers with high purity *via* an intrachain click cyclization.[22,23] To ensure the maintenance of the bromine terminus of the linear diblock copolymer prepared by consecutive ATRPs for the subsequent azidation, a low monomer conversion was used for both ATRP processes because of the previously reported successful ATRP production of polymers without any loss of highly reactive chain ends at low monomer conversions.[24] Following this synthesis guideline, *l*-P(OEGMA)-*b*-P(HEMA)-Br was thus synthesized at relatively low monomer conversions for both polymerization steps. Adoption of optimized reaction conditions for each polymerization step is supported by the kinetic studies (Fig. S2 and S3†).

*l*-P(OEGMA)-Br was first synthesized by ATRP of OEGMA using an alkynyl-terminated initiator.[25] All of the *l*-P(OEGMA)-Br synthesized at various polymerization times show a clear shift of the SEC elution peaks toward a greater molecular weight (MW) (shorter retention times) with unimodal and narrow-distributed MWs (Fig. S2a†). The degree of polymerization (DP) of *l*-P(OEGMA)-Br was calculated from the monomer conversion, which was determined by the $^1$H NMR analysis of unpurified reaction mixture. Taking 1.5 h of ATRP as an example (Fig. S1†), the monomer conversion was calculated to be 38.0% based on the following eqn (1), where $I_1$ and $I_2$ are the integrated intensity of the methylene protons in the polymerized OEGMA units and unpolymerized OEGMA monomer, respectively. The DP of *l*-P(OEGMA)-Br was thus 38 based on a target DP of 100. Next, *l*-P(OEGMA)-*b*-P(HEMA)-Br was prepared by ATRP of HEMA using *l*-P(OEGMA)$_{38}$-Br as a macroinitiator. Polymerization was conducted following the previously reported procedures with some modifications.[26] Note that a small amount of Cu(II) with a one quarter molar ratio to that of Cu(I) was added during polymerization to exert better modulation on the polymerization of HEMA and to minimize any chain termination reactions for the preservation of the terminal bromine group during the polymerization process considering the truly fast ATRP kinetics of HEMA. All of the *l*-P(OEGMA)-*b*-P(HEMA)-Br synthesized at various polymerization times show a clear shift of the SEC elution peaks toward a greater MW (shorter retention times) without any tailing at both high- and low-MW sides relative to the *l*-P(OEGMA)$_{38}$-Br

macroinitiator (Fig. S3a†), supporting the high initiation efficiency of P(OEGMA)-based macroinitiator for a well-controlled ATRP of HEMA. The living characteristics were reflected by the pseudo-first-order kinetics, an almost linear growth of MW with increased monomer conversion and narrow molecular weight distribution (Đ) recorded during the evaluated polymerization process (Fig. S3† and Table 1). The DP of the P(HEMA) block was calculated based on the following eqn (2), where $I_7$ is the integrated intensity of the terminal methyl protons in the side chain of OEGMA units, and $I_{10}$ is the integrated intensity of the hydroxyl protons of HEMA units (Fig. 1a). Because the P(HEMA) block was used for final CPT conjugation to serve as the hydrophobic moiety of the amphiphilic *cg*-prodrug, a diblock copolymer with the greatest hydrophilic weight fraction of the synthesized four polymer constructs, *i.e.*, *l*-P(OEGMA)$_{38}$-*b*-P(HEMA)$_9$-Br, was chosen for further reactions to guarantee sufficient colloidal stability for the self-assembled polymeric micelles. Therefore the linear precursor, *l*-P(OEGMA)$_{38}$-*b*-P(HEMA)$_9$-N$_3$, was prepared by azidation of the terminal bromine group with a 20-fold molar excess of sodium azide.[27,28]

$$\text{Conv.} = I_1/(I_1 + I_2) \times 100\%, \tag{1}$$

$$\text{DP of P(HEMA)} = 3I_{10}/I_7 \times 38. \tag{2}$$

*c*-P(OEGMA)$_{38}$-*b*-P(HEMA)$_9$ was later prepared by intrachain Cu(I)-catalyzed azide–alkynyl cycloaddition (CuAAc) of the linear precursor following reported procedures.[29] The cyclic diblock copolymer shows the same polymer composition as the linear precursor, as evidenced by the identical ratio of the integrated intensity of the OEGMA units to that of the HEMA units in the $^1$H NMR spectra (Fig. 1b). Successful cyclization was confirmed by a clear shift of the SEC elution trace of the synthesized cyclic copolymer toward a longer retention time (lower MW) as well as a discernible absence of the characteristic absorption band at ~2100 cm$^{-1}$ ascribed to the terminal azide group after cyclization compared to those of the linear precursor (Fig. S4†).

Multivalent pendant azide reactive sites for various potential functionalizations were introduced to the resulting cyclic diblock copolymer by esterification and subsequent azidation reactions of the hydroxyl groups of P(HEMA) with excessive iBuBr and sodium azide, respectively, to ensure the full transition, which is supported by the complete disappearance of the characteristic signal assigned to the hydroxyl group of HEMA units and the expected ratio of the integrated intensity
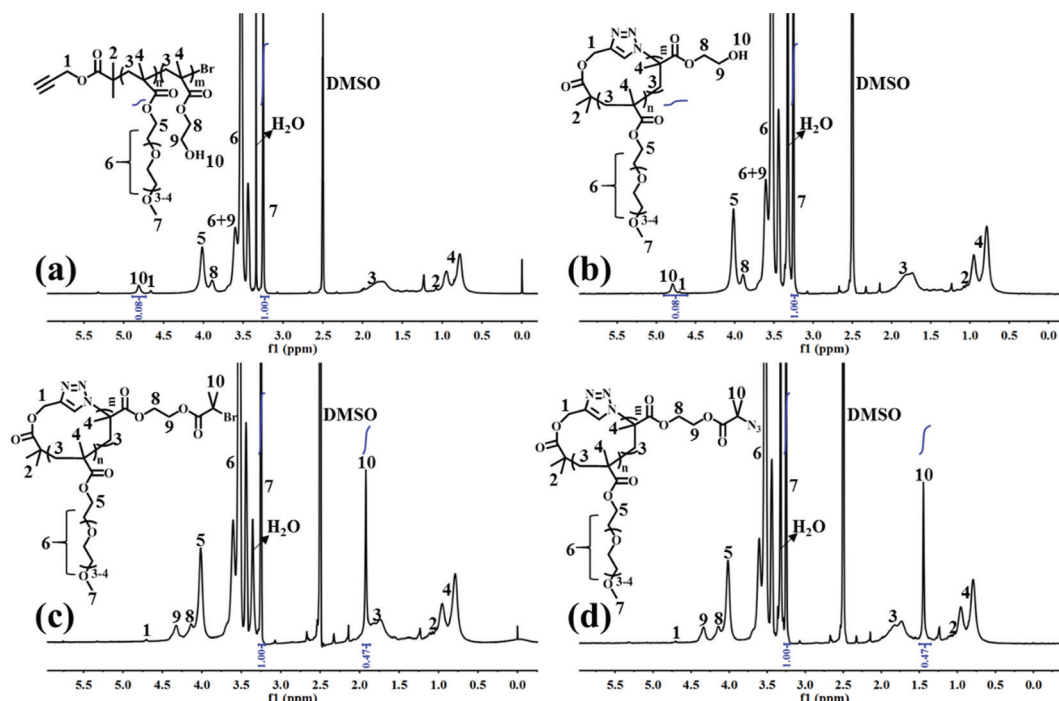
**Fig. 1** ¹H NMR spectra of (a) *l*-P(OEGMA)$_{38}$-*b*-P(HEMA)$_9$-Br, (b) *c*-P(OEGMA)$_{38}$-*b*-P(HEMA)$_9$, (c) *c*-P(OEGMA)$_{38}$-*b*-P(HEMA-Br)$_9$, and (d) *c*-P(OEGMA)$_{38}$-*b*-P(HEMA-N$_3$)$_9$ in DMSO-*d*$_6$.

of peak 10 ascribed to the methyl groups near bromine to that of peak 7 assigned to the pendant terminal methyl protons of the OEGMA units (Fig. 1c and d). *c*-P(OEGMA)$_{38}$-*b*-P(HEMA-Br)$_9$ and *c*-P(OEGMA)$_{38}$-*b*-P(HEMA-N$_3$)$_9$ (*cg*-N$_3$) share almost identical MW values, both of which are greater than that of *c*-P(OEGMA)$_{38}$-*b*-P(HEMA)$_9$ (Fig. S5a†).

Note that the use of an alkynyl-functionalized initiator in the consecutive two-step ATRP synthesis of *l*-P(OEGMA)-*b*-P(HEMA)-Br led to a partial occurrence of certain side reactions, including the addition of the generated radicals to the alkynyl terminus and Glaser coupling between the alkynyl termini, which produced a negligible portion of the high-molecular weight moiety in *l*-P(OEGMA)-*b*-P(HEMA)-Br, especially at the relatively low monomer conversions. However, further esterification of HEMA units with iBuBr contributed to a significant increase of the molecular weight of this part, resulting in the appearance of a small shoulder at high molar masses for both cyclic and linear polymers of P(OEGMA)-*b*-P(HEMA-Br).

Finally, alkynyl-SS-CPT was conjugated to *cg*-N$_3$ by intermolecular click coupling to yield the target *cg*-prodrug. The successful conjugation of CPT molecules is supported by recording a notable characteristic UV absorbance peak centered at 365 nm for *cg* and *bg*-prodrugs, which is almost identical to that of the free CPT molecules after the conjugation of CPT to *cg*-N$_3$ and *bg*-N$_3$ (Fig. 2), and by the appearance of a new signal at 7.6 ppm (peak 17) attributed to the proton of the click-formed triazole ring and the presence of CPT signals at 7.3–8.4 ppm (assigned to the aromatic protons) in the ¹H NMR spectra of the *cg*-prodrug (Fig. 3). More importantly, both *cg* and *bg*-prodrugs show unimodal and narrow-distributed MWs
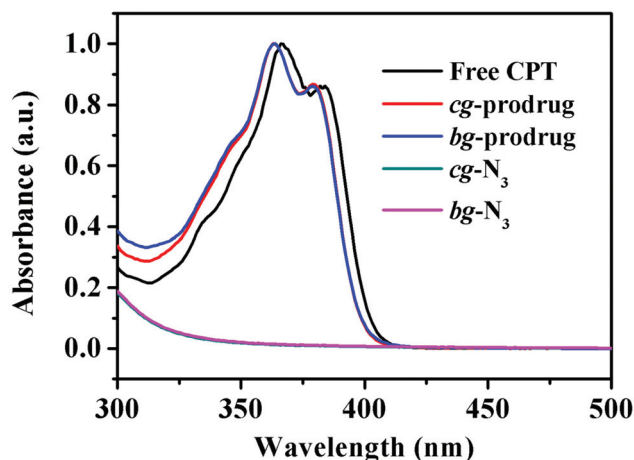


**Fig. 2** UV-vis spectra of free CPT, *cg*-N$_3$, *bg*-N$_3$, and *cg* and *bg*-prodrugs in DMSO.

(Fig. 4), confirming the successful preparation of the two prodrug formulations without any side reactions in the drug conjugation process.

The actual drug loading content (DLC) of *cg* and *bg*-prodrugs was determined to be 12.3% and 13.9%, respectively, by using a UV–vis spectrometer based on the standard calibration working curves (Fig. S11b†) and eqn (3), in which $m_{CPT}$ is the mass of the conjugated CPT that was calculated using the absorption measured by the UV–vis spectrometer, and $m_{cg-}$ or $_{bg-prodrugs}$ is the mass of *cg*- or *bg*-prodrugs, respectively. The theoretical DLC of *cg* and *bg*-prodrugs was calculated to be
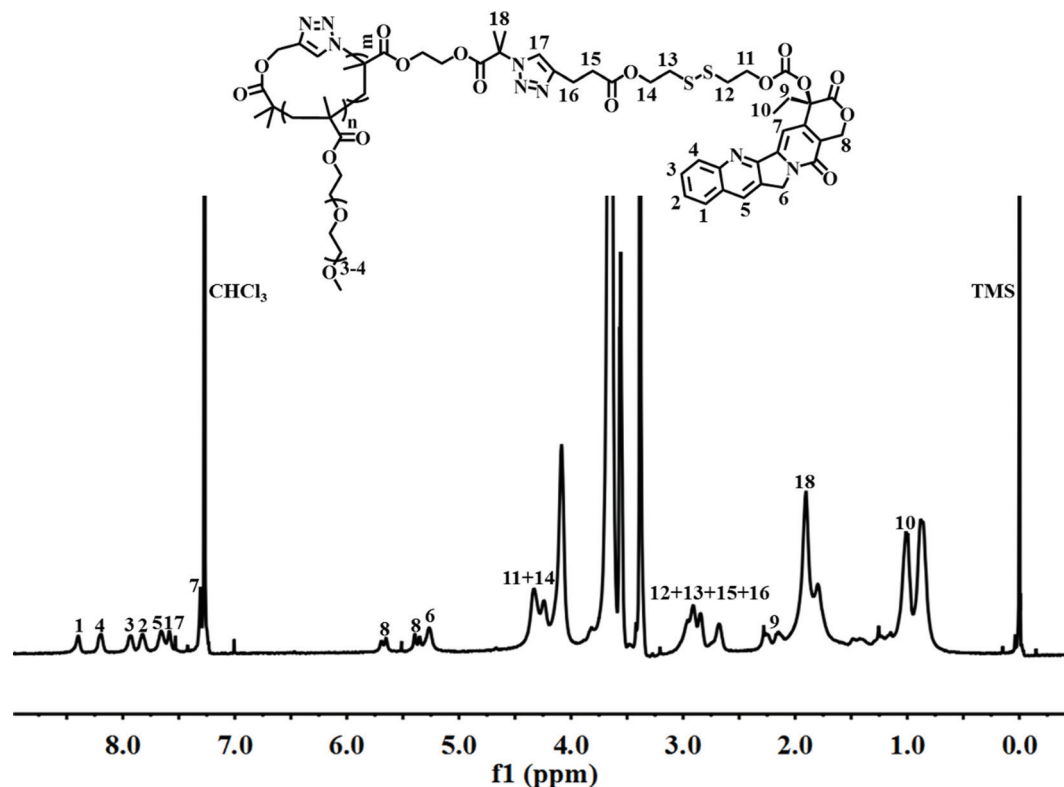
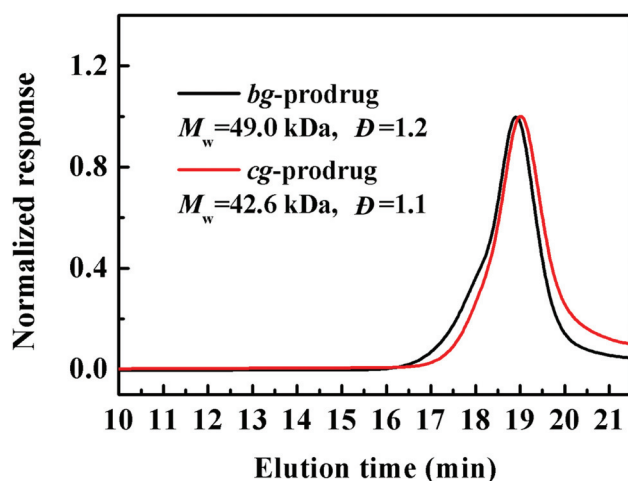**Fig. 3**  $^1$H NMR spectrum of *cg*-prodrug in CDCl$_3$.



**Fig. 4**  SEC elution traces of *cg* and *bg*-prodrugs.

16.3% and 17.4%, respectively, based on eqn (4) assuming the full occupation of the reactive azide functions by CPT molecules without any consideration of the negative effect resulting from the steric hindrance. In eqn (4), 348.35 is the molecular weight of CPT, and $n_{\mathrm{azide}}$ is the molar amount of azide functions in *cg* or *bg*-N$_3$. Therefore, the conjugation efficiency of CPT was finally determined by eqn (5) and all of the results are listed in Table 2. The slightly greater conjugation efficiency of the *bg*-prodrug than that of the *cg* analogue is reasonably attributed to the stronger steric hindrance of *cg* relative to *bg* formulations.[7]

$$\text{Actual DLC} = m_{\mathrm{CPT}}/m_{cg \text{ or } bg\text{-prodrugs}} \times 100\%, \qquad (3)$$

$$\text{Theoretical DLC} = 348.35 \times n_{\mathrm{azide}}/m_{cg \text{ or } bg\text{-prodrugs}} \times 100\%, \quad (4)$$

$$\text{Conjugation efficiency of CPT} = \text{actual DLC/theoretical DLC} \times 100\%. \qquad (5)$$

### Self-assembly behaviors of *cg* and *bg*-prodrugs

The critical micelle concentrations (CMCs) of both formulations were determined using pyrene as a fluorescent probe, and were determined to be 14.5 and 9.1 μg mL$^{-1}$ for *cg* and *bg*-prodrugs, respectively (Fig. S10†). The greater CMC value of the *cg*-prodrug relative to the *bg* analogue results likely from the different packing behaviors caused by the *cg* and *bg* copolymers with different topologies.[30–32] The cyclic polymers are entropically disfavored in the micellar state, because two block junctions must be located in the core–fringe interface in the micelles self-assembled from cyclic copolymers compared to the self-assembly behavior of *bg* copolymers with only one block junction.[7,22]

The micelles based on *cg* and *bg*-prodrugs with a final polymer concentration of 0.2 mg mL$^{-1}$ that is well above the CMC values for both formulations were next fabricated *via* a nanoprecipitation method by adding the polymer solution pre-

**Table 2** Summary of the calculated parameters of *cg* and *bg*-prodrugs

| Sample | Actual DLC (wt%) | Theoretical DLC (wt%) | Conjugation efficiency (%) | The number of CPT units | Polymer structure |
|---|---|---|---|---|---|
| *cg*-Prodrug | 12.3 | 16.3 | 75.5 | 6.8 | *cg*-P(OEGMA)$_{38}$-*b*-P(HEMA$_9$-SS-CPT$_{6.8}$) |
| *bg*-Prodrug | 13.9 | 17.4 | 79.9 | 8.0 | *bg*-P(OEGMA)$_{38}$-*b*-P(HEMA$_9$-SS-CPT$_{8.0}$) |

pared in DMSO dropwise into water followed by extensive dialysis against deionized water to remove any organic solvent. The mean size and size distribution (also termed as polydispersity index, PDI) of the two micelle prodrugs in an aqueous phase were determined by dynamic light scattering (DLS), which were found to be 52.2 nm and 0.22, and 64.9 nm and 0.19, respectively (Fig. 5a and b). The smaller size of micelles based on *cg*-prodrugs relative to micelles of *bg*-prodrugs is most likely attributed to the smaller dimension of the *cg*-prodrug than that of the *bg* construct that is supported by the SEC-MALLS-determined root-mean-square *z*-average radius of gyration, $\langle R_g \rangle$ value of *cg* (11.2 nm) and *bg* (15.1 nm)-prodrugs. Therefore, the results show that the dimension of both self-assemblies formed by the *cg* and *bg* polymers depends substantially on the molecular size of *cg* and *bg* polymers likely due to the steric hindrance of the grafted structures of *cg* and *bg* molecules and the relatively low aggregation number of the self-assembled structures. The salt stability of both micelle

prodrugs was next evaluated in PBS (pH 7.4, 150 mM). The apparent stability of both micelle constructs is supported by the almost identical size distribution upon a shift of the incubation media from water to PBS as well as an unaltered dimension during the assessed 30 days (Fig. 5a and b).

Transmission electron microscopy (TEM) observation was used to provide a morphological insight into the self-assembled nanoparticles formed by *cg* and *bg*-prodrugs. Both polymers can form well-dispersed micelles with a regular spherical shape. The mean diameter was estimated to be approximately 20 and 25 nm for micelles of *cg* and *bg*-prodrugs, respectively, based on the TEM observations (Fig. 5c and d). The smaller size visualized by TEM than that determined by DLS is attributed to the dehydrated status of TEM samples.[33,34]

To demonstrate the reduction-responsive degradation of micelles formed by *cg* and *bg*-prodrugs, the size change of both micelles incubated with 10 mM GSH was monitored by
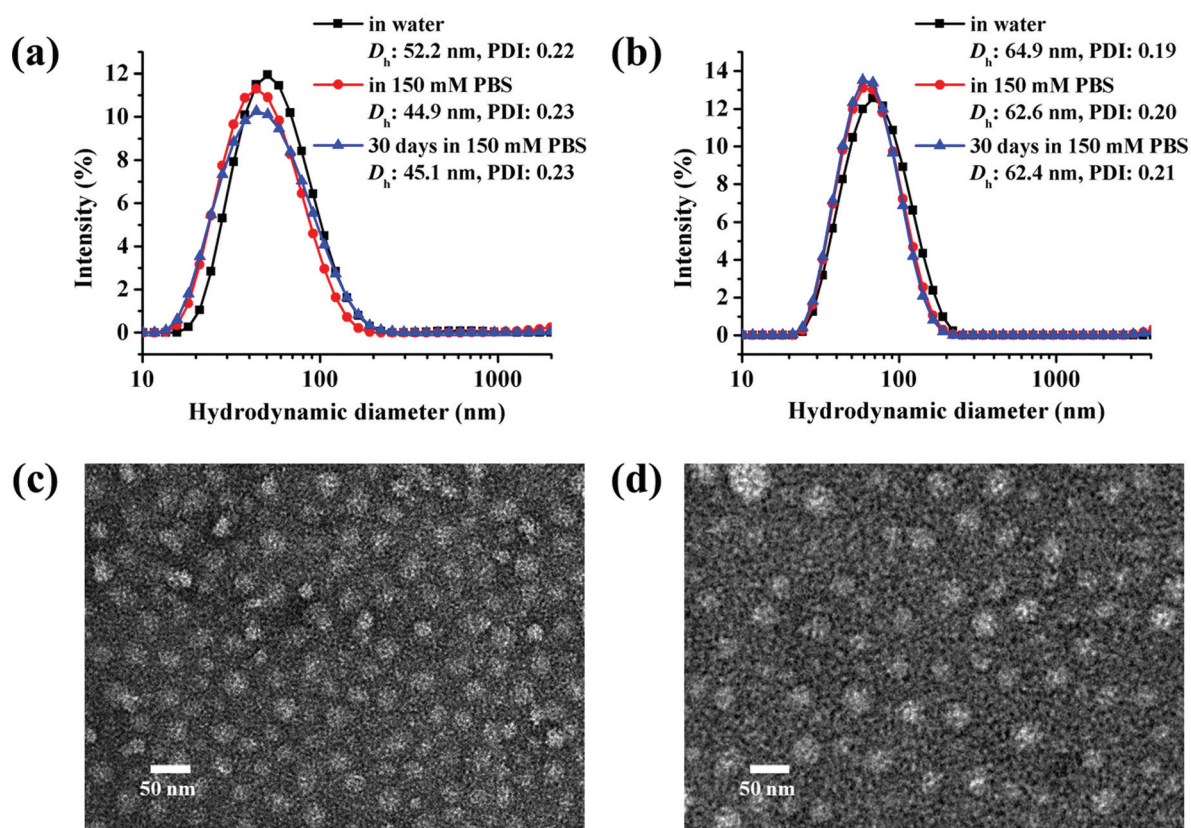


**Fig. 5** Size distributions and TEM images of micelles self-assembled by *cg* (a and c) and *bg*-prodrugs (b and d) at a fixed polymer concentration of 0.2 mg mL$^{-1}$.
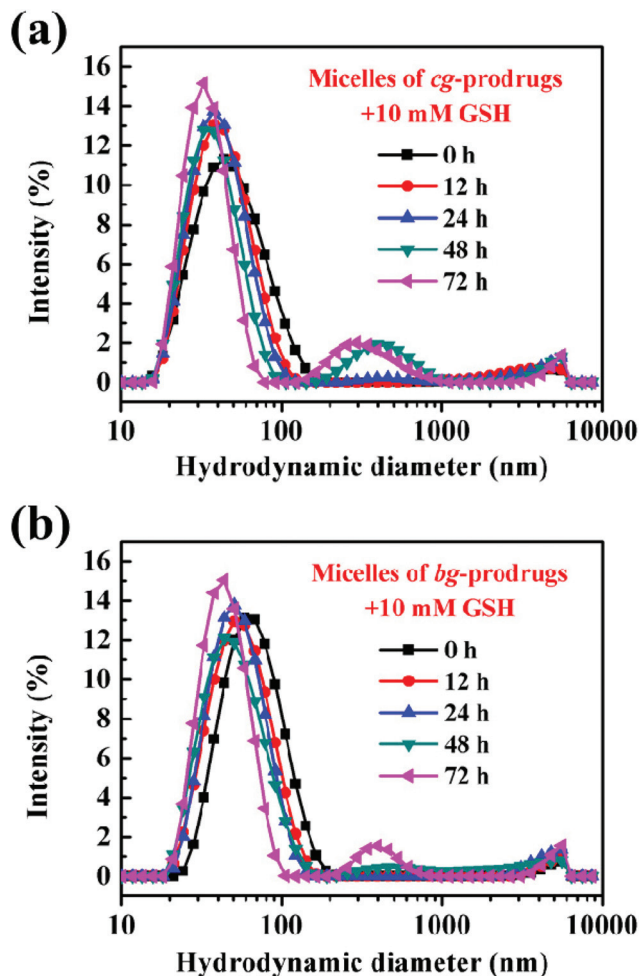
**Fig. 6** Reduction-triggered size changes of micelles based on *cg* (a) and *bg*-prodrugs (b) at various incubation periods with 10 mM GSH.



**Fig. 7** *In vitro* drug release profiles of micelles of *cg* and *bg*-prodrugs under different conditions at 37 °C.

DLS at different incubation intervals (Fig. 6). The unimodal size population centered at approximately 50 nm with a narrow distribution clearly evolved to the bimodal populations centered at around 40 and 400 nm with broad distributions for both micelles, which confirms the reduction-triggered cleavage of the disulfide link for CPT release from the parent micelle prodrugs[35–37] and the reassembly of the prodrug residues with greater hydrophilic weight fractions. Interestingly, the notable degradation of micelles based on *cg*-prodrugs commenced sometime after 12 h of incubation, which is faster than that of the *bg*-analogues with a starting time between 24 and 48 h. The lower DLC of *cg*-prodrugs seems to account substantially for the reduction-triggered promoted re-assembly process considering a speedier cleavage of low amounts of disulfide links by the consumption of the same amount of GSH.

### *In vitro* drug release study

To further validate reduction-sensitive drug release behaviors, an *in vitro* drug release study of micelles of *cg* and *bg*-prodrugs was investigated in PBS (pH 7.4, 150 mM) at 37 °C in the absence and presence of 10 mM GSH (Fig. 7). Both micelle
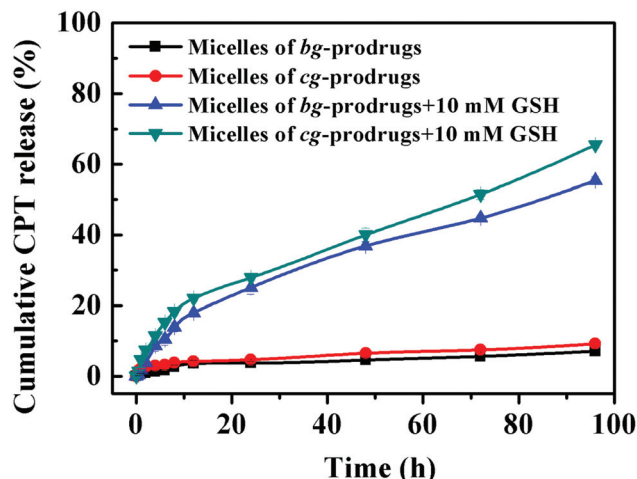
prodrugs had very good protection of the conjugated drug with less than 10% CPT release in 96 h without incubation of GSH because of the enhanced stability of the conjugated drug molecules for a minimized premature drug release and off-target associated side effects.[38] The slow hydrolysis of the carbonate bond in PBS likely accounts for the slight cumulative drug release in the absence of GSH.[39] However, incubation with 10 mM GSH significantly promoted CPT release to 65% and 55% for micelles of *cg* and *bg*-prodrugs in the same period, respectively, due to the reduction-triggered cleavage of CPT from the parent polymer. The faster drug release behaviors of *cg*-prodrug-based micelles than that of the micelles based on *bg* analogues agrees well with the faster degradation behaviors of the former micelle construct (Fig. 6).

### *In vitro* cellular uptake and cytotoxicity studies

To investigate the intracellular trafficking of *cg* and *bg*-prodrug-based micelles, the cellular uptake properties of the two micelle prodrugs with an equivalent CPT amount of 25 μg mL$^{-1}$ were visualized by fluorescence microscopy in HeLa cells. Note that the cells were stained with LysoTracker Green to distinguish from the blue fluorescence of CPT. The clear visualization of the overlapped blue and green colors in the merged images after 4 h of incubation (Fig. 8) confirms efficient endocytosis of both micelle formulations and the subsequent substantial localization of either micelle prodrugs or the released CPT molecules in the cytoplasm. The average fluorescence density per cell area of free CPT, micelles of *bg*-prodrugs, and micelles of *cg*-prodrugs was further determined to be 0.125, 0.088, and 0.095 per pixel, respectively, by semi-quantitative analysis of confocal images using ImageJ software. The cells treated with micelles of *cg* and *bg*-prodrugs presented weaker fluorescence intensity than those treated with free CPT due to their different internalization mechanisms (endocytosis *vs.* direct membrane permeation). The stronger fluorescence intensity of *cg*-prodrug-based micelles suggests the greater cellular uptake efficiency of this formulation than that of the *bg*-
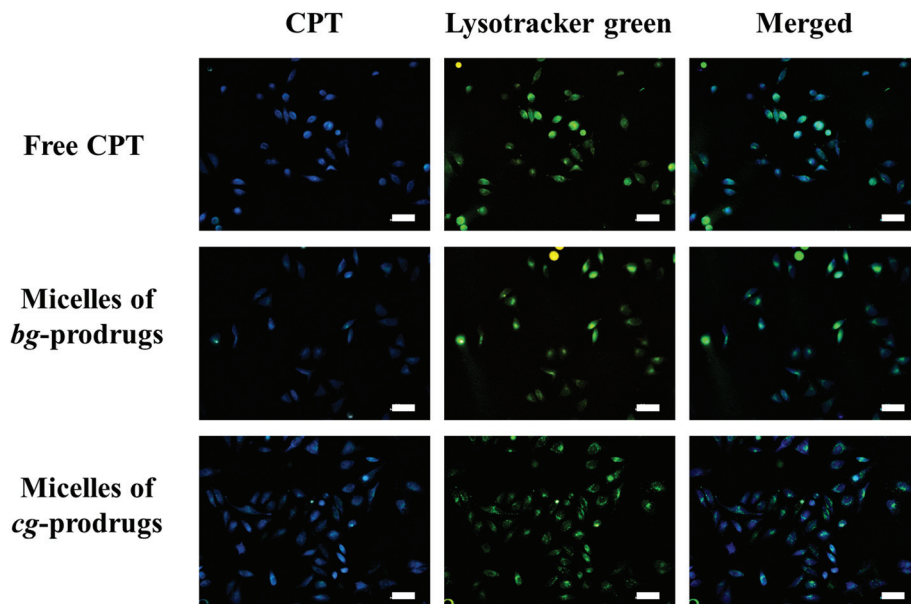
| | CPT | Lysotracker green | Merged |
|---|---|---|---|



**Fig. 8** Fluorescence images of HeLa cells incubated with free CPT and micelles of *bg* and *cg*-prodrugs for 4 h. The scale bars correspond to 50 μm in all the images.

based analogues. The cellular uptake efficiency was further quantified by flow cytometry (FCM) analysis (Fig. 9). The greater cellular uptake efficiency of the micelles of *cg*-prodrugs than that of the *bg*-prodrug-based analogues with statistical significance agrees well with the fluorescence observation, and is possibly attributed to the smaller size of the micelles of *cg*-prodrugs for faster and greater cellular internalization.[40]

Finally, *in vitro* cytotoxicity of *cg*-N$_3$, *bg*-N$_3$, and micelles of *cg* and *bg*-prodrugs was evaluated by a 3-(4,5-dimethylthiazol-2-yl)-5-(3-carboxymethoxyphenyl)-2-(4-sulfophenyl)-2*H*-tetrazolium (MTS) cell viability assay in HeLa cells (Fig. S12† and Fig. 10). Both polymer precursors, *cg*-N$_3$ and *bg*-N$_3$, were nontoxic to cells with a high viability above 90% at all the examined polymer concentrations. The half-maximal inhibitory concentration (IC$_{50}$) of free CPT, micelles of *cg*-prodrugs, and micelles of *bg*-prodrugs is determined to be 1.72 (1.31, 2.25), 3.96 (3.40, 4.61), and 5.35 (4.60, 6.22) μg mL$^{-1}$, respectively. Although both micelle prodrugs exhibited less *in vitro* cytotoxic activity than the free CPT likely due to their different internalization mechanisms mentioned above and the release kinetics of free drug from the micelle prodrugs, the micelle constructs with enhanced stability can prolong the blood circulation and
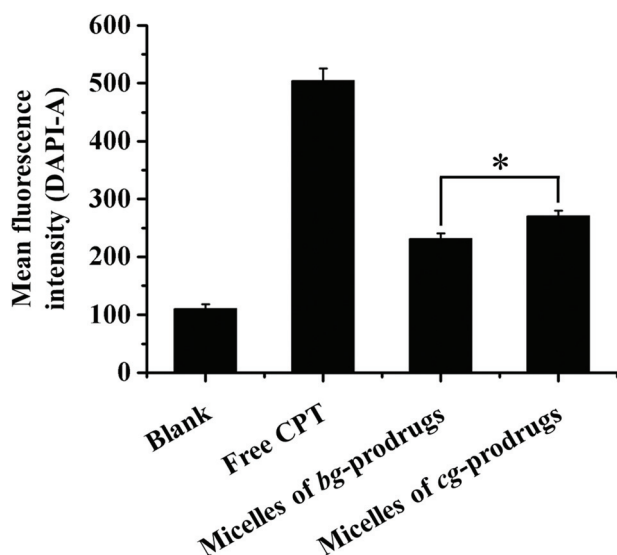


**Fig. 9** Quantitative measurements of the mean fluorescence intensity after incubation with free CPT and micelles of *bg* and *cg*-prodrugs in HeLa cells *via* flow cytometry analysis (4 h incubation, CPT concentration = 25 μg mL$^{-1}$, and 10 000 cells were counted). The data were expressed as mean ± SD, $n = 3$, Student's *t*-test, *$p < 0.01$.
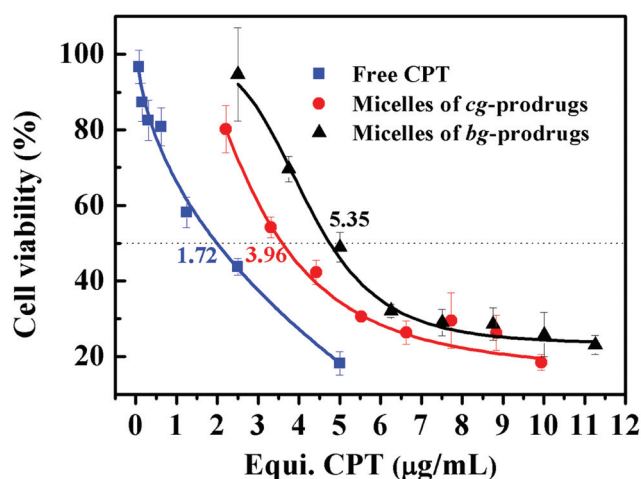


**Fig. 10** *In vitro* viability of HeLa cells treated with free CPT and micelles of *cg* and *bg*-prodrugs at various concentrations for 72 h of incubation.

enhance the passive accumulation of CPT molecules at the tumor site *via* an enhanced permeability and retention (EPR) effect as well as reduce the systematic side effects of free CPT. More importantly, *cg*-prodrug-based micelles exhibited greater cytotoxicity (lower $IC_{50}$ value) despite the lower DLC than the *bg*-based analogues, which results primarily from the faster reduction-triggered degradation and drug release as well as the greater cellular uptake efficiency of the former micelle prodrugs.

## Conclusions

In summary, we reported in this study the synthesis of *cg*-prodrugs with heterogeneous grafts of hydrophilic OEG and reducibly conjugated camptothecin (CPT) *via* an integrated strategy of a previously reported diblock copolymer-based template and post-polymerization intermolecular click conjugation of a reducible CPT prodrug to completely eliminate the compromised drug conjugation efficiency due to the steric hindrance of hydrophilic grafts. The micelles self-assembled from the *cg*-prodrugs had sufficient salt stability and reduction-triggered cleavage of the disulfide link for a promoted CPT release, simultaneously. Most importantly, we revealed that the dimension of both self-assemblies formed by the *cg* and *bg* polymers depends substantially on the molecular size of the *cg* and *bg* polymers and the *cg*-prodrug-based micelles exhibited greater *in vitro* cytotoxicity against cancer cells despite the lower DLC than the *bg*-based analogues. Therefore, the developed *cg*-prodrugs provide great potential for chemotherapy, and the aforementioned interesting results will definitely inspire more upcoming studies on the future design and development of novel *cg* polymers for biomedical applications.

## Conflicts of interest

The authors declare no competing financial interest.

## Acknowledgements

## References

1 L. Gao, Z. Ji, Y. Zhao, Y. Cai, X. Li and Y. Tu, *ACS Macro Lett.*, 2019, **8**, 1564–1569.
2 B. J. Ree, Y. Satoh, K. Sik Jin, T. Isono, W. Jong Kim, T. Kakuchi, T. Satoh and M. Ree, *NPG Asia Mater.*, 2017, **9**, e453–e453.
3 M. Schappacher and A. Deffieux, *Science*, 2008, **319**, 1512.
4 J. Yang, R. Wang and D. Xie, *Macromolecules*, 2019, **52**, 7042–7051.
5 F. Zhou, Z. Zhang, G. Jiang, J. Lu, X. Chen, Y. Li, N. Zhou and X. Zhu, *Polym. Chem.*, 2016, **7**, 2785–2789.
6 Y. Cheng, H. Wei, J.-K. Y. Tan, D. J. Peeler, D. O. Maris, D. L. Sellers, P. J. Horner and S. H. Pun, *Small*, 2016, **12**, 2750–2758.
7 Z. Liu, Y. Huang, X. Zhang, X. Tu, M. Wang, L. Ma, B. Wang, J. He, P. Ni and H. Wei, *Macromolecules*, 2018, **51**, 7672–7679.
8 X. Y. Tu, C. Meng, Y. F. Wang, L. W. Ma, B. Y. Wang, J. L. He, P. H. Ni, X. L. Ji, M. Z. Liu and H. Wei, *Macromol. Rapid Commun.*, 2018, **39**, 1700744.
9 B. Chen, K. Jerger, J. M. J. Fréchet and F. C. Szoka, *J. Controlled Release*, 2009, **140**, 203–209.
10 N. Nasongkla, B. Chen, N. Macaraeg, M. E. Fox, J. M. J. Fréchet and F. C. Szoka, *J. Am. Chem. Soc.*, 2009, **131**, 3842–3843.
11 M. C. Arno, R. J. Williams, P. Bexis, A. Pitto-Barry, N. Kirby, A. P. Dove and R. K. O'Reilly, *Biomaterials*, 2018, **180**, 184–192.
12 X. Y. Tu, C. Meng, X. L. Zhang, M. G. Jin, X. S. Zhang, X. Z. Zhao, Y. F. Wang, L. W. Ma, B. Y. Wang, M. Z. Liu and H. Wei, *Macromol. Biosci.*, 2018, **18**, 1800022.
13 S. Zhang, L. Yin, W. Zhang, Z. Zhang and X. Zhu, *Polym. Chem.*, 2016, **7**, 2112–2120.
14 S. Zhang, Y. Tezuka, Z. Zhang, N. Li, W. Zhang and X. Zhu, *Polym. Chem.*, 2018, **9**, 677–686.
15 B. Mu, Q. Li, X. Li, S. Pan, Y. Zhou, J. Fang and D. Chen, *Polym. Chem.*, 2016, **7**, 6034–6038.
16 R. J. Williams, A. Pitto-Barry, N. Kirby, A. P. Dove and R. K. O'Reilly, *Macromolecules*, 2016, **49**, 2802–2813.
17 C. E. Wang, H. Wei, N. Tan, A. J. Boydston and S. H. Pun, *Biomacromolecules*, 2016, **17**, 69–75.
18 H. Wei, C. E. Wang, N. Tan, A. J. Boydston and S. H. Pun, *ACS Macro Lett.*, 2015, **4**, 938–941.
19 X. Fan, G. Wang and J. Huang, *J. Polym. Sci., Part A: Polym. Chem.*, 2011, **49**, 1361–1367.
20 H. Zhang, W. Wu, X. Zhao and Y. Zhao, *Macromolecules*, 2017, **50**, 3411–3423.
21 L. Zheng, Y. Wang, X. Zhang, L. Ma, B. Wang, X. Ji and H. Wei, *Bioconjugate Chem.*, 2018, **29**, 190–202.
22 Z. Ge, Y. Zhou, J. Xu, H. Liu, D. Chen and S. Liu, *J. Am. Chem. Soc.*, 2009, **131**, 1628–1629.
23 L. Gao, J. Oh, T. Chang, D. Chen, X. Li, X. Yang, Y. Tu, X. Zhu and C. Y. Li, *Polymer*, 2016, **101**, 379–387.
24 J.-F. Lutz and K. Matyjaszewski, *J. Polym. Sci., Part A: Polym. Chem.*, 2005, **43**, 897–910.
25 D. Han, X. Tong, Y. Zhao, T. Galstian and Y. Zhao, *Macromolecules*, 2010, **43**, 3664–3671.
26 P. Yang and S. P. Armes, *Macromol. Rapid Commun.*, 2014, **35**, 242–248.
27 H. Wei, D. S. H. Chu, J. Zhao, J. A. Pahang and S. H. Pun, *ACS Macro Lett.*, 2013, **2**, 1047–1050.

28 X. Wan, T. Liu and S. Liu, *Biomacromolecules*, 2011, **12**, 1146–1154.

29 B. A. Laurent and S. M. Grayson, *J. Am. Chem. Soc.*, 2006, **128**, 4238–4239.

30 H. Iatrou, N. Hadjichristidis, G. Meier, H. Frielinghaus and M. Monkenbusch, *Macromolecules*, 2002, **35**, 5426–5437.

31 E. Minatti, P. Viville, R. Borsali, M. Schappacher, A. Deffieux and R. Lazzaroni, *Macromolecules*, 2003, **36**, 4125–4133.

32 G. E. Yu, Z. Yang, D. Attwood, C. Price and C. Booth, *Macromolecules*, 1996, **29**, 8479–8486.

33 X. Zhang, M. Zhang, M. Wang, H. Peng, Q. Hua, L. Ma, B. Wang and H. Wei, *Bioconjugate Chem.*, 2018, **29**, 2239–2247.

34 X. Zhang, X. Zhang, L. Sun, F. Liu, M. Wang, J. Peng, Y. Wang, L. Ma, B. Wang and H. Wei, *Chem. Commun.*, 2018, **54**, 13495–13498.

35 X. Hu, J. Hu, J. Tian, Z. Ge, G. Zhang, K. Luo and S. Liu, *J. Am. Chem. Soc.*, 2013, **135**, 17617–17629.

36 L. Dai, R. Cai, M. Li, Z. Luo, Y. Yu, W. Chen, X. Shen, Y. Pei, X. Zhao and K. Cai, *Chem. Mater.*, 2017, **29**, 6976–6992.

37 M. Hou, Y. E. Gao, X. Shi, S. Bai, X. Ma, B. Li, B. Xiao, P. Xue, Y. Kang and Z. Xu, *Acta Biomater.*, 2018, **77**, 228–239.

38 Y. Shen, E. Jin, B. Zhang, C. J. Murphy, M. Sui, J. Zhao, J. Wang, J. Tang, M. Fan, E. Van Kirk and W. J. Murdoch, *J. Am. Chem. Soc.*, 2010, **132**, 4259–4265.

39 S. J. Moon, S. V. Govindan, T. M. Cardillo, C. A. D'Souza, H. J. Hansen and D. M. Goldenberg, *J. Med. Chem.*, 2008, **51**, 6916–6926.

40 T. Chang, M. S. Lord, B. Bergmann, A. Macmillan and M. H. Stenzel, *J. Mater. Chem. B*, 2014, **2**, 2883–2891.